High-Pressure Study of Adamantane: Variable Shape Simulations up to 26 GPa

N. Arul Murugan,[†] R. S. Rao,[‡] S. Yashonath,*[,†] S. Ramasesha,[†] and B. K. Godwal[‡]

Solid State and Structural Chemistry Unit, Indian Institute of Science, Bangalore 560 012, India, and High Pressure Physics Division, Purnima Laboratories, BARC, Mumbai 400085, India

Received: June 29, 2005; In Final Form: July 13, 2005

We report simulations of adamantane by carefully combining ab initio and empirical approaches to enable simulations with internal degrees of freedom on crystalline adamantane up to a pressure of 26 GPa. Two sets of simulations, assuming the adamantane molecule as a rigid (RB) and flexible body (FB), have been carried out as a function of pressure up to 26 GPa to understand changes in the crystal structure as well as molecular structure. The flexible body simulations have been performed by including 6 lowest frequency internal modes (obtained from DFT calculations performed with Gaussian98) out of the total of 72. The calculated variation in c/a and V/V_0 from the RB and FB calculations as a function of pressure have been compared with the experimental curve. Other relevant thermodynamic and structural properties reported are the radial distribution functions, deviation in the position of a given type of atom with respect to its position at standard pressure, δ_s, cell parameters, volume, and energy. With an increase in pressure, three additional peaks are seen to develop gradually at three different pressures in the center of mass (com)−com radial distribution function (rdf). We attribute these changes to structural transformations (probably second-order phase transitions) which is consistent with the three phase transitions reported by Vijayakumar et al. for adamantane in the pressure range of 1 atm−15 GPa. Our simulations also show that these additional peaks in the rdf's are associated with the differences between opposite and parallel spin neighbors of Greig and Pawley as well as the crystallographic directional dependence of intermolecular distances in the first three shells of the neighbors. Also, the structural quantities from the RB calculation show considerable deviation from the FB calculation for pressures greater than 5 GPa, which suggests that the rigid body assumption for molecules may not be valid above this pressure.

1. Introduction

Adamantane ($C_{10}H_{16}$) is a highly symmetric molecule with point group symmetry, T_d. A cagelike structure is formed with six CH_2 and four CH groups giving rise to a molecular structure with four cyclohexane rings in chair form. This structure has zero strain as all C−C−C bond angles are 109.45°. While there exists a large number of experimental and theoretical studies of molecules such as fullerenes[1−3] under extreme pressures, simpler caged molecular systems such as adamantane or hexamethylene tetramine have hardly been explored under extreme pressures. Vijayakumar et al.[4,5] and Rao et al.[6] have recently reported experimental investigations on the behavior of the equation of state of adamantane up to 26 GPa. Their X-ray diffraction and Raman measurements indicate the possibility of several phase transitions in this range of pressure. These studies along with those of Steiner and Saenger[7] suggest a gradual decrease in the nonbonded H−H distance from 2.48 Å to a limiting value of 1.9 Å. At these rather short internuclear distances it is expected that the contribution of H−H interactions will be repulsive. Phase transitions or changes in the nature of the bonding are expected to relieve these repulsive interactions. There is evidence that the phase transition at 0.5 GPa is brought about by a similar mechanism; the H−H distance shows an increase from 2.23 Å at 0.1 MPa to 2.37 Å above 0.5 GPa. It therefore appears that under further compression adamantane may undergo intramolecular deformation leading to polymerization, decomposition, amorphization, or disorder in H positions.

In recent times, adamantane has attracted much attention especially at high pressures. Under extreme pressures, these are expected to form diamond. A number of properties of adamantane and adamantane derivatives have been experimentally measured at ambient pressures and pressures up to 5 GPa. Molecular simulations have been extensively used to study the transitions from tetragonal ordered phase to plastic crystal cubic phase as well as the nature of disorder in the plastic crystal phase[8−10] as a function of temperature at ambient pressure.

In these simulations, a classical intermolecular potential function has been employed as is the common practice. Such a description remains adequate when no significant changes in molecular geometry occur. Experimental investigations of Vijayakumar et al.[4,5] suggest that beyond 8.0 GPa significant distortion of the molecular geometry takes place. Under these circumstances the usual approach cannot be employed. However, first principle calculations with more than a few molecules is beyond the computational capability of even supercomputers, while a purely classical description is inadequate. To overcome these difficulties, we retain advantages of employing a classical potential but include internal degrees of freedom to permit molecular distortion. This has been achieved through a novel combination of classical Monte Carlo simulations and ab initio Gaussian98[11] calculations on adamantane.

Gaussian98 calculations were performed on a single molecule of adamantane. Complete optimization of the molecule is carried

* To whom correspondence should be addressed. E-mail: yashonat@sscu.iisc.ernet.in.
† Indian Institute of Science.
‡ Purnima Laboratories.

10.1021/jp053542h CCC: $30.25
Published on Web 08/18/2005

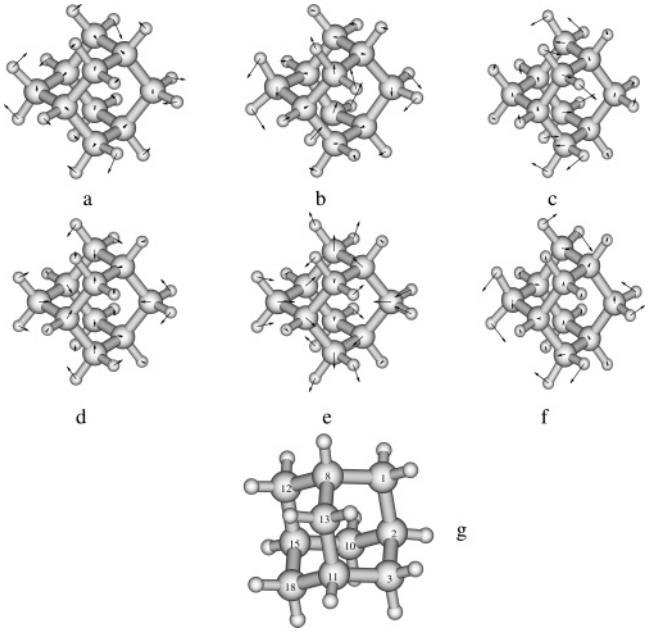

Figure 1. Six low-frequency normal modes (a) $\nu = 342.3025$ cm^{-1}, (b) $\nu = 342.7428$ cm^{-1}, (c) $\nu = 342.7428$ cm^{-1}, (d) $\nu = 416.4384$ cm^{-1}, (e) $\nu = 416.4477$ cm^{-1}, and (f) $\nu = 460.0101$ cm^{-1} in increasing order of the frequency along with the displacement vectors are shown and (g) labeling employed for the atoms.

out with density functional calculations (DFT) using Becke three-parameter method and Lee−Yang−Parr electron correlation functional with 6-31G(d) basis. There are in all 72 normal modes, of these many are high-frequency modes which do not distort easily and hence they need not be included in the present calculation. We have chosen to include six of the lowest frequency modes. The nature of motion or molecular distortion associated with these modes is shown in Figure 1.

Metropolis Monte Carlo simulations employing a variable shape simulation cell in the isothermal−isobaric ensemble have been carried out including the motion associated with the six internal degrees of freedom. These calculations have been carried out up to a pressure of 26.0 GPa. Radial distribution functions, equation of state, nature of molecular distortion, and properties which give information about molecular distortion are reported. The results confirm the existence of more than one phase transition.

2. Methods

2.1. Intermolecular Potential. Intermolecular interactions between adamantane have been accounted in terms of short range (6-exp) pair potential between sites with one site on each of the C and H atoms. We have chosen the potential of Greig and Pawley.[8] Greig and Pawley[8] employed the potential originally proposed by Williams.[12] As previous work has demonstrated,[13,14] the parametrization of Williams generally overestimates the overall intermolecular interaction energy of the crystal. For example, it was found that benzene did not exhibit rotation around the C_6 axis in the room temperature phase although the NMR work of Andrew and Eades[15] showed that such rotation does occur. Thus, there are three important effects of the use of such strongly bound potential: (i) The crystal appears to be more strongly bound than found experimentally. (ii) The resulting dynamics of both translational and reorientational motion is slower in the crystal. (iii) Another effect of this is that the transition temperature is generally higher than that expected.

TABLE 1: Potential Parameters for Adamantane

type	*A*, kJ/mol Å^6	*B*, kJ/mol	*C*, Å^{-1}
C−C	2156.4	326792.2	3.60
C−H	474.7	34959.2	3.67
H−H	103.5	10639.7	3.74

In fact, this is confirmed in the previous studies on adamanatane using the potential by Williams. Greig and Pawley found that the molecular dynamics study of crystal to plastic crystal transformation in adamantane occurs around a temperature of 410 K which is much higher than the experimentally observed transition temperature (208.62 K). Our own recent study[14] of the transition between the ordered and disordered phases as a function of temperature as well as pressure using the intermolecular interactions of Greig and Pawley suggests similar trends.

Clearly, a modification to correct this anomaly is essential. The potential due to Greig and Pawley has the form

$$u_{\mathrm{kl}} = -\frac{A}{r^6_{\mathrm{kl}}} + B\exp(-Cr_{\mathrm{kl}}) \tag{1}$$

with one interaction site located on each of the C and H atoms.

Here we have reduced the depth of C−C, C−H, and H−H interaction potentials by 10% to correct for overestimation of the binding. The parameters *A*, *B*, and *C* were originally obtained by Williams[12] by fitting to a number of compounds containing C and H. As Williams has noted[12] the Coulombic interactions have only marginal contribution and therefore no charges have been placed at the atomic sites. These potential parameters which were later modified by Greig and Pawley[8] for their simulations are tabulated in Table 1. We have chosen to use this potential as results for this model have been reported by Greig and Pawley[8] and provide a good reference for comparison.

The intermolecular interaction energy, U_{inter} is defined as

$$U_{\mathrm{inter}} = \frac{1}{2N}\sum_{i=1}^{N}\sum_{j=1}^{N}\sum_{k=1}^{N_a}\sum_{l=1}^{N_b} u_{kl,ij}(r_{kl,ij}) \tag{2}$$

2.2. Intramolecular Interactions. We have carried out density functional calculations using the Becke three-parameter method and Lee−Yang−Parr electron functional with 6-31G-(d) basis set with the help of Gaussian98[11] on an isolated adamantane molecule. Of all the normal modes, the lowest frequency modes are likely to be important as they would correspond to displacements with low effective force constants. We have chosen to include six of the lowest frequency normal modes in the Monte Carlo calculations. The displacement vectors and the nature of these modes are shown in Figure 1. The intramolecular strain energy associated with a given mode is given by

$$u_{\mathrm{intra},j} = \frac{1}{2}\sum_{i}^{3N} k_j Q_i^2 \tag{3}$$

where Q_i are the normal coordinates, *N* refers to the number of atoms, and k_j refers to the force constant of *j*th mode.

The total intramolecular energy is

$$U_{\mathrm{intra}} = \sum_{j=1}^{3N-6} \phi_j u_{\mathrm{intra},j} \tag{4}$$

where ϕ_j is the weighting factor associated with the *j*th mode.

Table 2 lists the frequencies of the normal modes as well as the force constants for each of the six modes.

TABLE 2: Six Low-Frequency Modes and Their Corresponding Force Constants

	ν, cm^{-1}	force constant, mdyne/A	symmetry
1	342.3025	0.1401	*B*
2	342.7428	0.1406	*B*
3	342.7428	0.1406	*A*
4	416.4384	0.4867	*A*
5	416.4477	0.4868	*A*
6	460.0101	0.2238	*A*

2.3. NPT-MC Simulations. Simulations have been carried out in an isothermal−isobaric or NPT ensemble with a variable shape simulation[16] cell using the Monte Carlo method and the importance sampling algorithm of Metropolis et al.[17] The simulation cell is represented by 6 degrees of freedom in contrast to the 9 degrees original used (see below) while 12 degrees of freedom are associated with each molecule: 3 with translation, 3 with rotation, and 6 with the internal modes. Thus, the average of any property a is obtained by integrating over these $(12N + 9)$ variables

$$\langle a \rangle = \frac{\int \mathrm{d}\mathbf{a}\, \mathrm{d}\mathbf{b}\, \mathrm{d}\mathbf{c}\, \mathrm{d}\Omega^N \prod_{i=1}^{6} \mathrm{d}\mathbf{d_i^N}\, \mathrm{d}\mathbf{r}^N a(\mathbf{r}^N,\Omega^N,\phi^N) p(\mathbf{r}^N,\Omega^N,\phi^N)}{\int \mathrm{d}\mathbf{a}\, \mathrm{d}\mathbf{b}\, \mathrm{d}\mathbf{c}\, \mathrm{d}\Omega^N \prod_{i=1}^{6} \mathrm{d}\mathbf{d_i^N}\, \mathrm{d}\mathbf{r}^N p(\mathbf{r}^N,\Omega^N,\phi^N)} \quad (5)$$

where $p(\mathbf{r}^N,\Omega^N,\mathbf{d_i^N}, \bar{\mathbf{a}}, \bar{\mathbf{b}}, \bar{\mathbf{c}}) = \mathrm{e}^{-\beta U(\mathbf{r}^N,\Omega^N,\mathbf{d_i^N}, \bar{\mathbf{a}}, \bar{\mathbf{b}}, \bar{\mathbf{c}})}$ and $a(\mathbf{r}^N,\Omega^N,\mathbf{d_i^N}, \bar{\mathbf{a}}, \bar{\mathbf{b}},\bar{\mathbf{c}})$ are the probability and the property, respectively, for each configuration specified by $(\boldsymbol{r}^N,\Omega^N,\boldsymbol{d_i^N})$. Here, the $\mathbf{r}^N$ values are the center of mass positions of the molecules, and Ω^N values specify the orientations of molecules as a whole, while $(\bar{\mathbf{d}}_1, \bar{\mathbf{d}}_2, \bar{\mathbf{d}}_3, \bar{\mathbf{d}}_4, \bar{\mathbf{d}}_5, \bar{\mathbf{d}}_6)^N$ specifies six internal vibrations of the N molecular species. Note that $\boldsymbol{r}$ and Ω have three components each: $\boldsymbol{r}$ specifies the three Cartesian coordinates and Ω the three Euler angles. Variable shape simulation cell was employed as it provides the necessary degrees of freedom for the simulation cell to be in any one of the crystal systems. The simulation cell is represented by three vectors, the cell vectors, **a**, **b**, and **c**. Parrinello and Rahman[16] originally chose the three vectors without any constraints. The cell vectors contribute nine additional degrees of freedom. However, as Yashonath and Rao[18] showed subsequently, only six degrees of freedom are necessary for representing the simulation cell. These could be, for example, the typical cell parameters a, b, c, α, β, and γ. The three additional degrees of freedom in the original formulation of Parrinello and Rahman[16] often lead to rotation of the simulation cell[18] as a whole especially in polyatomic systems, which is not desirable. This can be overcome by reducing the nine degrees of freedom to the essential six by choosing vector **a** along the x-axis, **b** in the xy-plane, and **c** in any direction. Such a choice does not limit or prevent the system from undergoing solid−solid-phase transformation from one space group to another. Thus, the simulation involves integration over $(12N + 6)$ degrees of freedom. In systems such as biphenyl[19] or stilbene[20] the amplitude of the torsional mode involving the torsional displacement of the two phenyl rings is comparable to the molecular translation or rotation modes. And in the case of molecules under high pressure, the distortion in molecular geometry is such that the amplitude of low-frequency normal modes is comparable to the amplitude of rotational or translational motions.

3. Computational Details

Two different sets of simulations have been carried out. In the first set referred to as RB simulation no internal modes are included. The molecule is kept as a rigid unit. In the second set, 6 of the 72 internal degrees of freedom have been included. These are referred to as FB simulations.

The starting configuration for the simulation at 1 atm and 188 K is taken from the X-ray diffraction structural details provided by Amoureux and Foulon.[21] The structure with the space group $P\bar{4}2_1c$ has two molecules per unit cell and has cell parameters $a = b = 6.639$ Å, $c = 8.918$ Å, and $\alpha = \beta = \gamma = 90°$ at 188 K. We have observed in our earlier calculations that the complete transition to an orientationally ordered phase from a disordered phase requires very long equilibration. As our aim is to understand the high-pressure phase starting with the ambient-pressure phase, we start with an orientationally ordered phase. The initial state for a high-pressure simulation is prepared as follows: Initial simulation at 188 K and 1 atm of pressure is carried out starting with an experimental crystal structure. Then a second simulation starting with the final configuration of this simulation is carried out at 1.0 GPa and 188 K. Starting with the final configuration of this simulation, we carry out a simulation at 1.0 GPa and 300 K. The phase has been observed to be tetragonal during all these simulations. Starting with this final phase, we have carried out simulations by gradually increasing the pressure up to 26.0 GPa as well as by decreasing the pressure up to 0.1 MPa (1 atm of pressure).

All the simulations are carried out with 128 molecules in $4 \times 4 \times 4$ unit cells. Each MC move consists of an attempt to displace each of the N molecules once[22,23] followed by a rotation of the molecule as a whole through an axis chosen randomly and rotated by a random angle whose maximum value is chosen so as to obtain about 40% acceptance probability. In the case of FB calculations, the MC move additionally involves displacement of the normal coordinate, whose unit vector is shown in Figure 1, for the six chosen modes. The displacement magnitude along the normal coordinate for each of the modes is chosen randomly. In a given MC move, only one of the six normal modes is selected randomly for an attempted displacement. A MC move also consists of an attempt to modify one of the three cell vectors defining the simulation cell.[18] Thus, each MC step consists of N molecular center of mass displacements, N rotations of the molecule as a whole, N normal mode displacements one for each molecule, and a single cell vector displacement. We have carried out simulations for a total of 26 000 MC moves which include 6000 MC moves for equilibration. We found that the energy and other properties converged within the first 3000 MC steps. After the equilibration, various average structural quantities such as cell parameters, volume, and radial distribution functions have been calculated.

4. Results and Discussion

Variation of c/a ratio in the tetragonal phase over 0.0−26.0 GPa is shown in Figure 2a for RB and FB simulations. Also shown are the experimental data points obtained from the X-ray data.[4,5] The value of c/a for FB simulation of adamantane with six internal modes is closer to the experimental value up to 8.0 GPa. In contrast, RB calculations show poor agreement to the experimental variation of c/a with pressure.

Beyond 8.0 GPa, the experimental variation with pressure is more gradual. By 10.0 GPa it is seen that the experimental curve is closer to the RB simulations. There is no experimental data beyond 13.0 GPa, and hence it is difficult to determine whether the RB or the FB are more realistic.

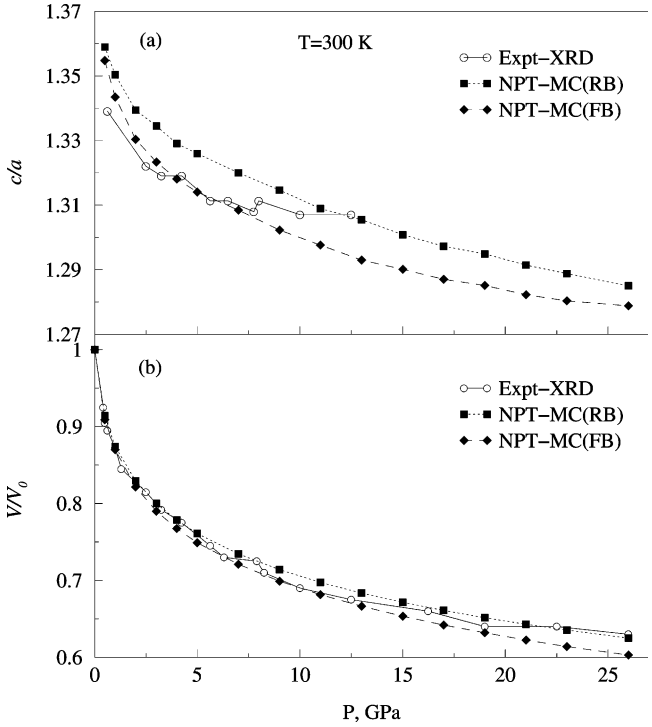

Figure 2. (a) Calculated and experimental c/a variation as a function of pressure. The calculated values are for both RB and FB models. (b) Calculated V/V_0 values for both RB and FB and experimental V/V_0 variations as a function of pressure.

Before we comment on the implications of these findings, let us look at the variation of V/V_0 with pressure. The equation of state of adamantane at 300 K is shown in Figure 2b. Experimental values of V/V_0 against pressure are also shown. Below 5.0 GPa there is little difference between the RB and FB as well as the experimental curves. Beyond 5.0 GPa and up to about 12.0 GPa, the FB model describes the experimental variation better than the RB model. Beyond 15.0 or 20.0 GPa the variation of the RB model is closer to the experimental curve.

In summary, the FB model describes the variation in c/a and V/V_0 quite accurately only up to about 8−12.0 GPa. Note that these pressures are quite large, and one cannot rule out significant changes in both intramolecular and intermolecular distances and angles. The fact that the FB model describes the variation in c/a and V/V_0 better than the RB model clearly suggests that at these pressures distortion of the molecular geometry is already taking place. Later, we shall present direct evidence in support of this model. The absence of such internal degrees of freedom permitting distortion of the molecule at these pressures in the case of the RB model is responsible for the poor agreement of the c/a and V/V_0 with the experimental data.

Beyond 12.0 GPa, we find that the agreement of the experimental curve, where available V/V_0 is better with the RB and not the FB model. This is surprising since one expects that the distortions permitted in the case of the FB model should have resulted in better agreement of the two properties, c/a and V/V_0, with the experimental curve for this model and not for the RB model. However, to understand this result, one needs to understand the effect of increasing pressure on the molecular geometry. At lower pressures, internal modes of adamantane with lower force constants are involved. In contrast, at higher pressures, internal modes of adamantane with relatively higher force constants become increasingly important as the force on the molecule is significant. Thus, for lower applied pressures, it is to be expected that the distortions that take place in the molecular geometry arise from those associated with the low-frequency internal modes. As the applied pressure increases, the high-frequency internal modes become increasingly important. The distortion in molecular geometry at higher pressures is associated with these high-frequency modes.

TABLE 3: Internal Modes of Adamantane in Different Frequency Range and Their Degeneracy

range of ν, cm^{-1}	degeneracy	range of ν, cm^{-1}	degeneracy
300−400	3	1000−1200	11
400−500	5	1200−1500	16
500−800	4	1500−1600	6
800−900	4	>3000	16
900−1000	7		

The reasonable agreement of the FB model up to a pressure of around 8−12 GPa indicates that the six low-frequency modes with frequencies less than 446 cm^{-1} are actually adequate to describe the changes up to this pressure. They suggest that higher frequency modes, those between 446 and 3065 cm^{-1} are necessary to describe the changes in the c/a and V/V_0 values. In Table 3 we list the number of modes in different ranges of frequencies. There are altogether 72 modes with some frequencies beyond 3000 cm^{-1}. It is to be expected that at a pressure of 26 GPa, modes of frequencies as high as 1000 cm^{-1} ($460 \times 26/12 = 997$) will be important. However, even modes of higher frequencies might be involved. From Table 3, this means that 23 internal modes need to be included to obtain good agreement with the experimental quantities.

The agreement of the c/a at around 12.0 GPa and V/V_0 at a pressure beyond 20.0 GPa obtained from the RB model with the experimental curve is due to fortuitous cancellation of errors. At high pressures, experiments have shown unambiguously that distortions in the geometry of the adamantane molecule occur.

Other reasons for poor agreement of the FB model with the experiment at higher pressures might be due to (i) inaccuracies in the intermolecular potential (which was derived based on structures of solid at low pressures) and (ii) the harmonic potential that we have used (see eq 3). At higher pressures, the distortions are large and anharmonicities might be important.

Variation of a, b, and c with pressure up to 26.0 GPa is shown in Figure 3 for RB and FB models. Unfortunately, no experimental values are available for comparison. A smaller decrease in c/a is seen from experiments which suggests a smaller reduction in c as compared to a. In our calculations we find a slightly larger change in c as compared to a. The c value decreases from 9.5 to 7.5 Å when pressure is increased from 1.0 to 26.0 GPa. In comparison, a decreases from 6.68 to 5.58 Å over the same pressure range. As expected, the FB model undergoes larger changes in the lattice parameters than those in the RB model.

We show the variation of intermolecular interaction energy (U_{inter}) as a function of pressure in Figure 4a; U_{inter} exhibits a minimum between 0.5 and 1.0 GPa and thereafter increases with the increase in pressure. The minimum at low pressure is attained as the molecules in the crystal rearrange giving rise to better packing. Indeed, the minimum in U_{inter} appears to be associated with the transition from an orientationally disordered phase to an ordered phase. It appears that once transition into an ordered phase occurs any further increase in pressure leads only to an increase in U_{inter}. This is consistent with the experimental studies of Vijayakumar et al.[4,5] and Rao et al.[6] who find that the H−H distance decreases from 2.4 to 1.9 Å reflecting larger steric repulsions. The most favorable H−H interaction takes place at a distance of around 2.4 Å. The repulsive interaction at still higher pressure leads to change in

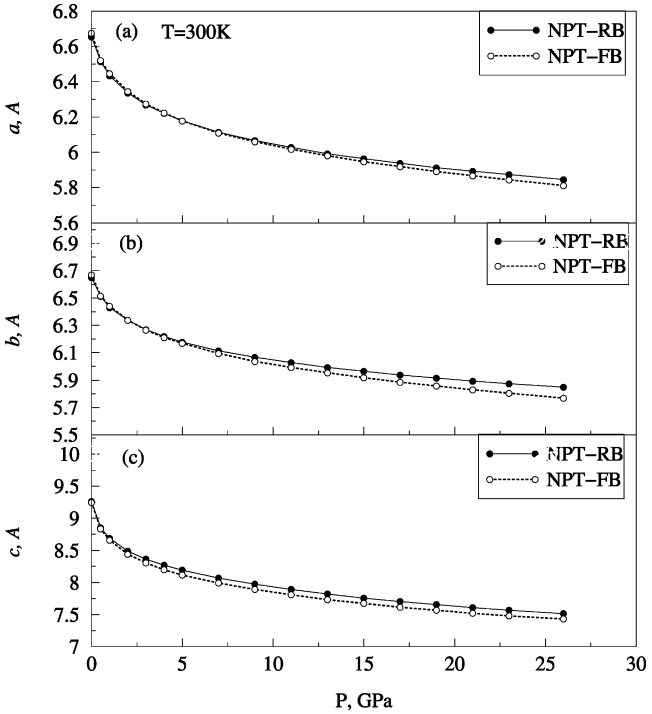

Figure 3. Variation of cell parameters as a function of pressure for both RB and FB models: (a) the "*a*" parameter, (b) the "*b*" parameters, and (c) the "*c*" parameter.

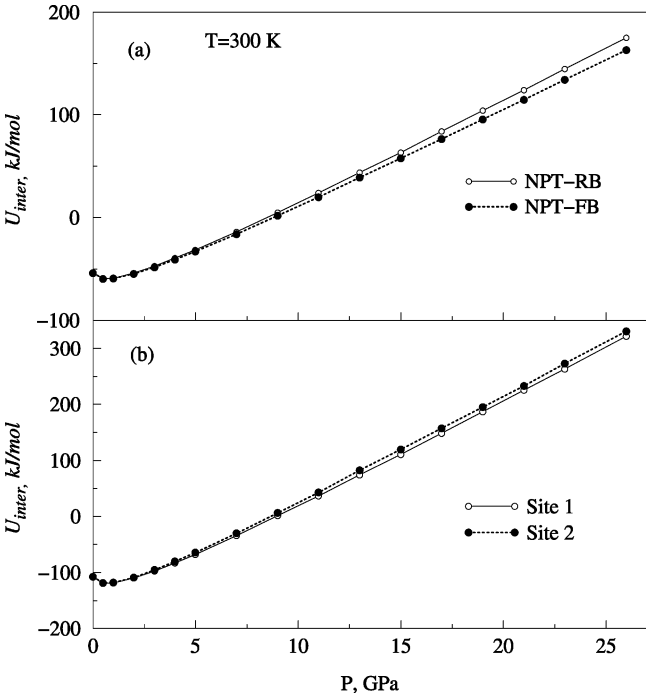

Figure 4. (a) Variation of intermolecular interaction energy, U_{inter}, as a function of pressure for RB and FB models. (b) U_{inter} as a function of pressure averaged over site 1 and site 2 separately.

CH vibrational line shape and the CH stretching modes as Raman[6] and IR[24] measurements have shown and eventually to distortion of molecular geometry. From Figure 4a we see that beyond 9.0 GPa, U_{inter} contributes positively to the total interactions. This pressure seems to be associated with a reversible phase transition seen around 8.5 GPa. Existence of this reversible transition was arrived at by Rao et al. from a Raman scattering study of pressure dependence of internal mode frequencies of adamantane.[6]

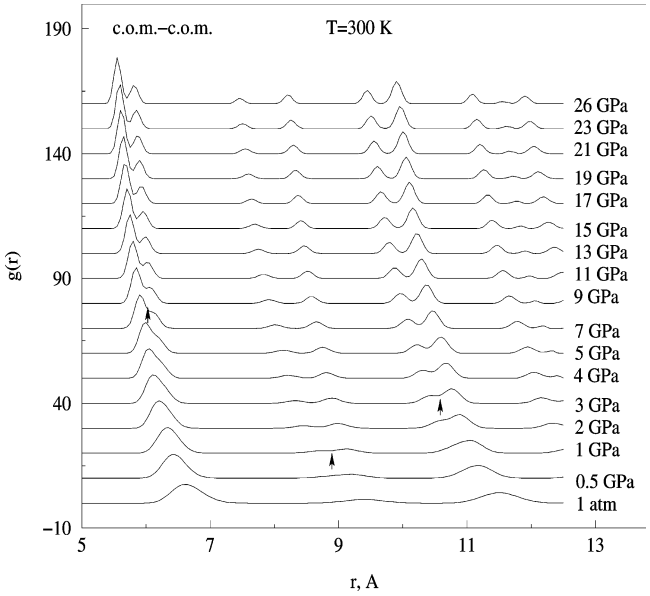

Figure 5. Plot of com−com rdf as a function of pressure for the FB model.

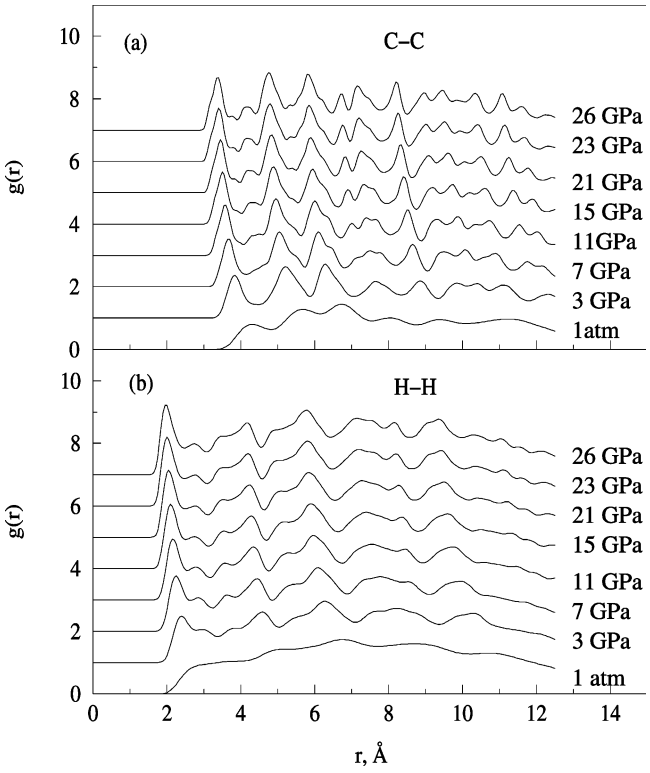

Figure 6. (a) C−C rdf and (b) H−H rdf as a function of pressure for the FB model.

Center of mass (com)−com, C−C, and H−H rdf's are plotted in Figures 5 and 6, respectively, up to 12.5 Å for pressure ranging from 1 atm to 26.0 GPa. A gradual shift of the observed peaks toward lower *r* values is evident with increase in pressure. Further, additional peaks appear at certain pressures. The peaks appear gradually suggesting that structural change is not of first order but probably second order. This is more clearly evident in the com−com rdf. Figure 7 shows com rdf's on an expanded scale at a few chosen pressures and chosen peaks where changes occur. Note that the abscissa of the com rdf at lower pressure has been scaled by the ratio, ρ_H/ρ_L, where ρ_H and ρ_L are the densities at high and low pressures, respectively. This takes into

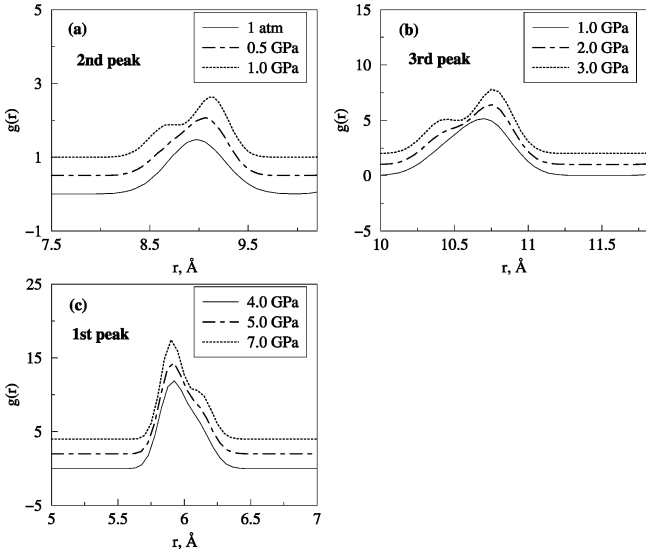

Figure 7. Plot of com−com rdf's at different pressures *after* a shift of the rdf in proportion to the relative density ratio for comparison to see the emergence of additional peaks.

TABLE 4: Interpretation of the First Six Peaks in the Center of Mass−Center of Mass Radial Distribution Function

neighbor	range of *r*, Å[a]	number of neighbors	crystallographic direction	spin[b]
1	5.3−5.7	8	[111]	opposite
2	5.7−6.1	4	[010]	parallel
3	7.0−7.7	2	[001]	parallel
4	7.7−8.6	4	[110]	parallel
5	9.0−9.6	8	[011]	parallel
6	9.6−10.3	16	[131]	opposite

[a] The different shifts to lower distances on increase in pressure is consistent with the different relative contribution of *c*. [b] The opposite or parallel orientation of neighbors with respect to the central adamanatane molecule is according to Greig and Pawley.[8]

account the shift in the position of the peak to lower distance as a consequence of the change in density with increase in pressure.

Each of the three peaks at 1 atm in the com−com rdf split into 2 peaks by 7 GPa. Additional peaks from the fourth shell can also be seen at higher pressures due to an increase in density. To understand the reasons for the appearance of three new peaks in the rdf from the existing three peaks at lower pressures, we attempted to assign neighbors in the crystal lattice responsible for these peaks. We shall refer to the position of the peaks in the rdf at 26 GPa. Table 4 gives the direction of the location of the neighbor for different peaks obtained from the analysis of the 298 K, 26 GPa structure along with the molecular orientation (parallel or opposite, up or down spin). Note that the first peak around 5.5−5.7 Å is comprised of eight neighbors located in the crystallographic [111] direction. The second peak (5.7−6.1 Å) consists of four neighbors located in [100] and [010] family of directions (see Figure 8). Note that in the analysis of Pawley and Greig,[8] they pointed out that among the 12 first shell neighbors,[14] 8 are first neighbors with antiparallel spin (with molecular orientation opposite to that of the molecule at the center) while the remaining 4 are of parallel spin or orientation. We see that under pressure these spins or molecules with opposite or parallel orientation shift by different amounts. The reason for these different amounts of shift may be understood when we note that with increasing pressure, the ratio *c*/*a* decreases from 1.34 at 1 atm to 1.29 at 26 GPa. As the [111] direction has a *c* component, the decrease in *r* for these eight

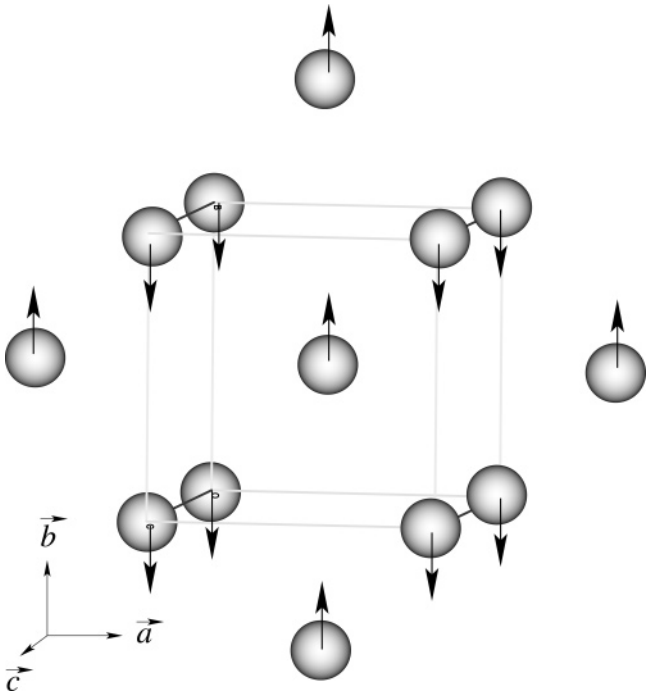

Figure 8. Neighbors contributing to the first peak in com−com rdf at 1 atm are shown with their spins. Of the 12 neighbors, 8 are along [111] and have opposite "spins" while the other 4 are along [100] with "spins" parallel.

neighbors is larger than that for the four neighbors which are along the [100] and [010] directions. The third peak (7.0−7.7 Å) has just two neighbors in [001] direction while the fourth peak is along the [110] direction. As the third peak has no components in any direction other than *c*, the shift is maximum for this due to a decrease in *c*/*a* ratio with pressure. The decrease in the distance with pressure at which the fourth peak is seen is smaller. The fifth peak (between 9 and 9.6 Å) along the [011] and [101] directions having components with 8 neighbors (parallel spins) along the *c* direction shifts by a larger amount as compared to the sixth shell (9.7−10.3 Å, 16 neighbors, antiparallel spins) along the [111] direction. This is not surprising as the latter has contributions from both the *a* and *b* axes (in addition to *c*) whereas the former has contributions from *c* apart from *a*. We also would like to point out that the resolution of the peaks at high pressures has contributions from the reduced, restricted thermal motion around the equilibrium position of various atoms of the three shells. The shifts are due to an increase in density.

In summary, the relative shifts of the various peaks seem to be determined by not so much the parallel or antiparallel orientation or spins but the directions along which they are located. The decrease in the ratio *c*/*a* suggests a larger decrease in *c* as compared to *a* upon increase in pressure. Therefore, those neighbors which have components along *c* show greater shifts to lower values of *r* as compared to neighbors which have either a smaller contribution from *c* or no contribution from *c* at all. It is unlikely that molecular distortions play a significant role in these shifts in the intermolecular distances.

Figure 9a gives the variation of the position at which the peaks in the com−com rdf are seen. Three new peaks in com−com rdf may be seen. The first new peak appears around 1.0 GPa at 8.8 Å, and the second peak around 10.7 Å develops into two distinct peaks between the pressure range 2.0−3.0 GPa. Between 5.0 and 7.0 GPa, a shoulder is seen to the right of the first peak around 6.2 Å.

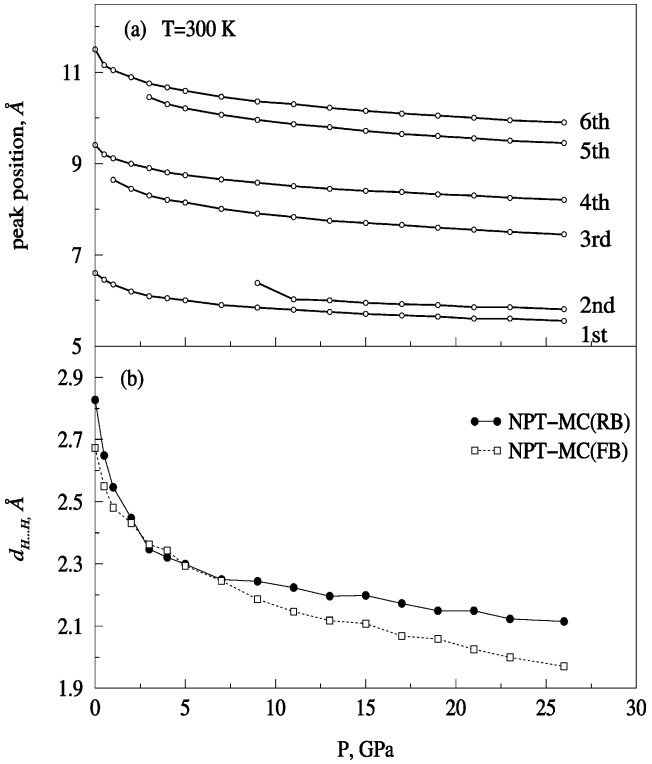

Figure 9. (a) Variation of the peak positions in com−com rdf as a function of pressure and (b) Variation of the shortest intermolecular H−H distance as a function of pressure for both RB and FB models.

The variation of the intermolecular H−H distance is shown in Figure 9b. The distance decreases from 2.8 Å at 1 atm to about 2.15 Å at 10.0 GPa for the flexible adamantane. This may be compared with the decrease obtained experimentally by Rietveld refinements using angle dispersive X-ray powder diffraction measurements. They found that the H−H distance decreases to 1.9 Å by about 10.0 GPa. In obtaining the H−H distance from Rietveld refinements, it was assumed that the crystal remains in the tetragonal phase without undergoing any change in crystal structure. If this assumption is valid, then it appears that our model may require a lowered H−H repulsion term saturating at a shorter distance. In other words, both the well depth and the distance at which the well depth reaches a minimum need to be reduced. For Lennard-Jones form, this means that both σ and ϵ should be reduced. If on the other hand, adamantane undergoes a transition to another structure, then the variation obtained from Rietveld refinements may not be correct. More careful experiments are required to verify if there is any transition or molecular distortion below 10.0 GPa.

To understand the nature of distortion taking place in the molecular geometry at these pressures, we show the shift in the position of the various carbon atoms (secondary as well as tertiary) with respect to the molecular center of mass in Figure 10. These positional shifts have been obtained after averaging over both the crystallographic sites 1 and 2 in the originally chosen tetragonal unit cell. Specifically, the shifts, $\delta_s(P)$, are defined as the change in the distance between the given atom i (with the center of mass as the origin) relative to its value at 1 atm

$$\Delta\bar{r}_{i,c}(P) = \bar{r}_i(P) - \bar{r}_{\mathrm{com}}(P) \tag{6}$$

$$\delta_s(P) = \Delta\bar{r}_{i,c}(P) - \Delta\bar{r}_{i,c}(1\ \mathrm{atm}) \tag{7}$$

The shift in the tertiary carbons are seen to be small. The

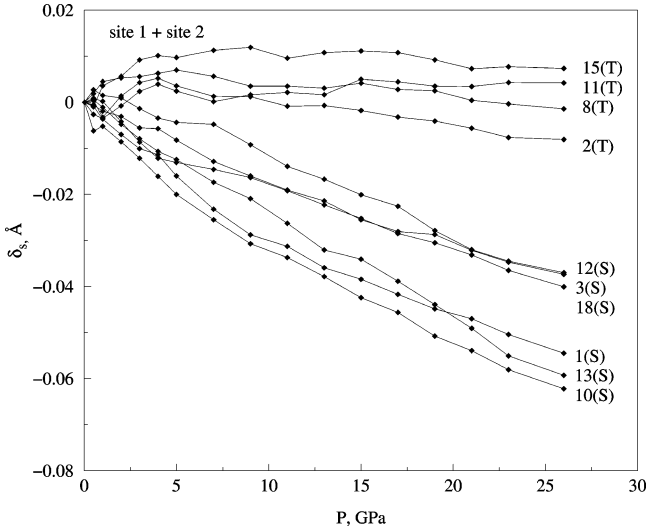

Figure 10. Variation of δ_s as a function of pressure.

secondary carbons, in contrast, show greater shifts. The negative shift implies that the atoms are closer to their respective molecular com as compared to their position at 1 atm of pressure. The shifts are toward their molecular com by distances ranging from 0.03 to 0.06 Å. Three of the six secondary atoms show larger shifts while the other three show smaller shifts.

To arrive at a more detailed picture, in Figure 11 we show the shifts for the adamantane molecule at crystallographic site 1 and site 2 separately. Note that the shifts and therefore distortions are quite different for the molecule at site 1 compared to that at site 2. While site 1 exhibits a distortion in which the tertiary carbons move away from their respective com's, secondary carbons approach closer to the com. The distortion here can be visualized as follows. The tertiary carbons form a tetrahedra while the secondary carbons form an octahedra. The distortion is so as to expand the tetrahedra but contract the octahedra.

The distortion of the site 2 molecule suggests that all the atoms are closer to their respective com. However, the nature of distortion is similar in that the approach of the tertiary carbons toward the com is less than that of the secondary carbons. In other words, here the distortion is such that both the octahedra formed by the secondary carbons and the tetrahedra formed by the tertiary carbons are squeezed upon an increase in pressure.

To see why there is a difference in the behavior δ_s with pressure for molecules at site 1 and site 2, we computed the lattice energy of a molecule at site 1 and site 2. Variation of this energy with pressure is shown in Figure 4b. Note that the energy is lower (larger in magnitude) for site 1. The differences between the energies at site 1 and site 2 are small at low pressures. However, at high pressures, this increases and becomes significant. This shows that site 1 and site 2 are nonequivalent, and they experience a different environment. This appears to affect the response to pressure leading to different kinds of molecular distortion at the two crystallographic sites. Experiments are required to verify these predictions. A further refinement in these calculations can be achieved by including a larger number of internal modes. Such studies will provide a more accurate estimate of different properties. By including the distortion of molecules in site 1 and site 2 (during the refinement of crystallographic structure) on the basis of our calculations, it is possible to get more accurate structural data for adamantane at higher pressures.

The variation of the C−C−C bond angles for tertiary and secondary carbon atoms with pressure are shown in Figure 12.

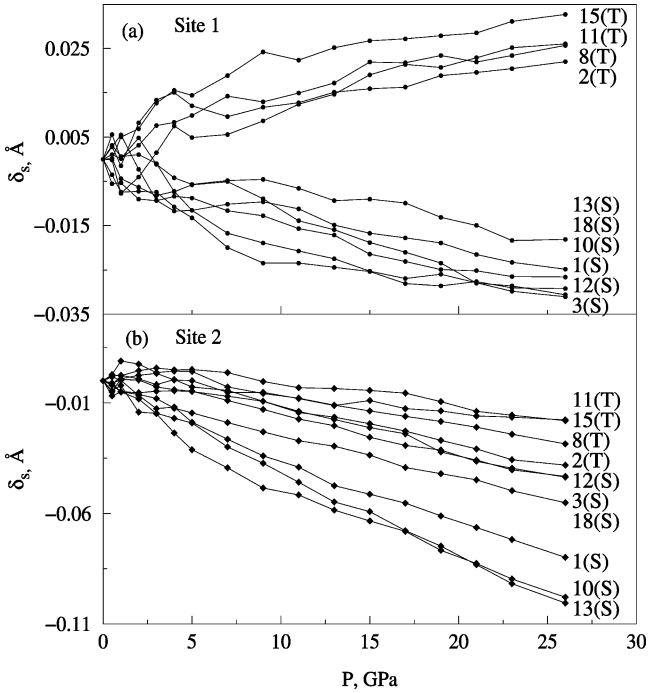

Figure 11. Variation of δ_s as a function of pressure averaged over (a) site 1 and (b) site 2 molecules.

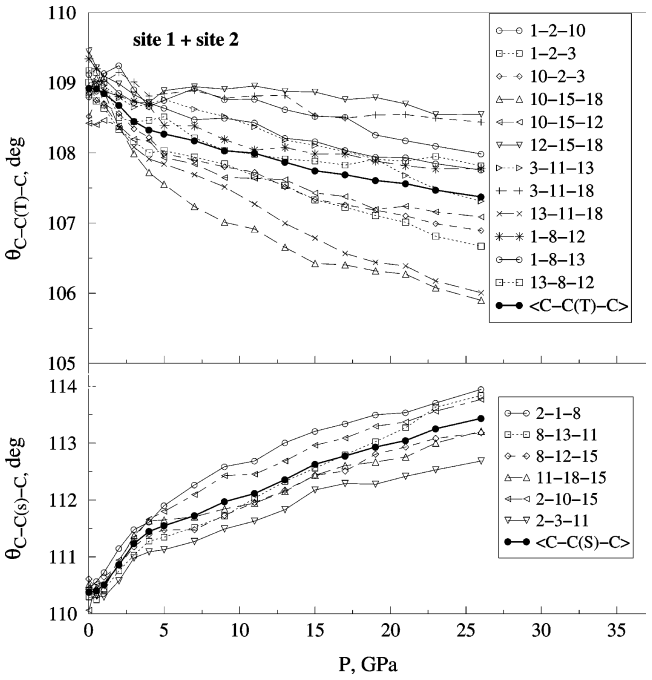

Figure 12. Bond angle variation as a function of pressure, averaged over all the molecules (a) C−C(T)−C and (b) C−C(S)−C.

Note that the C−C−C angle at the secondary carbons increase on the application of pressure while the tertiary carbons decrease with an increase in pressure. These are consistent with the behavior of δ_s values with pressure.

4.1. Conclusions. Variable shape simulations up to 26.0 GPa have been carried out for adamantane using both RB and FB assumptions for molecules. Both models predict the c/a and V/V_0 variations as a function of pressure. In the case of calculations with FB model cell parameters, H−H intermolecular contact and volume variation show larger changes as a function of pressure. Appearance of three new peaks in the com−com rdf at the pressure ranges between 0.5 and 1.0 GPa, 2.0−3.0 GPa, and 5.0−7.0 GPa may be compared to the three phase transitions reported in the pressure range 1 atm−15.0 GPa by Vijayakumar et al.,[4,5] Rao et al.,[6] and Steiner and Saenger[7] through their neutron diffraction studies and Raman/IR measurements. Also, the molecular distortion as a function of pressure has been looked at in detail. The molecules in site 1 and site 2 are affected by the pressure in different ways.

Acknowledgment. The authors wish to thank Department of Science & Technology, New Delhi, and BRNS, Mumbai, for financial support. The authors also wish to thank Dr. V. Vijayakumar for fruitful discussions.

References and Notes

(1) Shirl, M.; Breitline, M.; Jones, A. D.; Boyd, R. H. *J. Chem. Phys.* **1971**, *54*, 3959.
(2) Snoke, D. W.; Raptis, Y. S.; Syassen, K. *Phys. Rev.* **1992**, *45*, 1419.
(3) Chandrabhas, N.; Sood, A. K.; Muttu, D. V. S.; Sunder, C. D.; Bharathi, A.; Hariharan, Y.; Rao, C. N. R. *Phys. Rev. Lett.* **1994**, *73*, 3411.
(4) Vijayakumar, V.; Garg, A. B.; Godwal, B. K.; Sikka, S. K. *Chem. Phys. Lett.* **2000**, *10*, 275.
(5) Vijayakumar, V.; Garg, A. B.; Godwal, B. K.; Sikka, S. K. *J. Phys.: Condens. Matter.* **2001**, *13*, 1961.
(6) Rao, R.; Sakuntala, T.; Deb, S. K.; Roy, A. P.; Vijayakumar, V.; Godwal, B. K.; Sikka, S. K. *J. Chem. Phys.* **2000**, *112*, 6739.
(7) Steiner, T.; Saenger, W. *Acta Crystallogr.* **1991**, *B47*, 1022.
(8) Greig, D. W.; Pawley, G. S. *Mol. Phys.* **1996**, *89*, 677.
(9) Trew, A. S.; Pawley, G. S. *Can. J. Chem. Phys.* **1988**, *66*, 1018.
(10) Ciccotti, G.; Ferrario, M.; Memeo, E.; Meyer, M. *Phys. Rev. Lett.* **1987**, *59*, 2574.
(11) Frisch, M. J.; Trucks, G. W.; Schlegel, H. B.; Scuseria, G. E.; Robb, M. A.; Cheeseman, J. R.; Zakrzewski, V. G.; Montgomery, J. A., Jr.; Stratmann, R. E.; Burant, J. C.; Dapprich, S.; Millam, J. M.; Daniels, A. D.; Kudin, K. N.; Strain, M. C.; Farkas, O.; Tomasi, J.; Barone, V.; Cossi, M.; Cammi, R.; Mennucci, B.; Pomelli, C.; Adamo, C.; Clifford, S.; Ochterski, J.; Petersson, G. A.; Ayala, P. Y.; Cui, Q.; Morokuma, K.; Malick, D. K.; Rabuck, A. D.; Raghavachari, K.; Foresman, J. B.; Cioslowski, J.; Ortiz, J. V.; Stefanov, B. B.; Liu, G.; Liashenko, A.; Piskorz, P.; Komaromi, I.; Gomperts, R.; Martin, R. L.; Fox, D. J.; Keith, T.; Al-Laham, M. A.; Peng, C. Y.; Nanayakkara, A.; Gonzalez, C.; Challacombe, M.; Gill, P. M. W.; Johnson, B. G.; Chen, W.; Wong, M. W.; Andres, J. L.; Head-Gordon, M.; Replogle, E. S.; Pople, J. A. *Gaussian 98*, revision A.9; Gaussian, Inc.: Pittsburgh, PA, 1998.
(12) Williams, D. E. *J. Chem. Phys.* **1967**, *47*, 4680.
(13) Yashonath, S.; Price, S. L.; McDonald, I. R. *Mol. Phys.* 1988, *64*, 361.
(14) Murugan, N. A.; Yashonath, S. *J. Phys. Chem.* **2005**, *B109*, 2014.
(15) Andrew, E. R.; Eades, R. G. *Proc. R. Soc.* **1953**, *A218*, 537.
(16) Parrinello, M.; Rahman, A. *Phys. Rev. Lett.* **1980**, *45*, 1196.
(17) Metropolis, N.; Rosenbluth, A. W.; Rosenbluth, M. N.; Teller, A. H.; Teller, E. *J. Chem. Phys.* **1953**, *21*, 1087.
(18) Yashonath, S.; Rao, C. N. R. *Chem. Phys. Lett.* **1985**, *22*, 119.
(19) Murugan, N. A.; Jha, P. C.; Yashonath, S.; Ramasesha, S. *J. Phys. Chem.* **2004**, *B108*, 4178.
(20) Murugan, N. A.; Yashonath, S. *J. Phys. Chem.* **2004**, *B108*, 17403.
(21) Amoureux, J. P.; Foulon, M. *Acta Crystallgr.* **1987**, *B43*, 470.
(22) Normand, J.-M. *A Lie Group: Rotations in Quantum Mechanics*; Elsevier: 1981.
(23) Allen, M. P.; Tildesley, D. J. *Computer Simulation of Liquids*; Clarendon Press: Oxford, U.K., 1987.
(24) Salmon, D.; Shannon, V. L.; Strauss, H. L. *J. Chem. Phys.* **1989**, *90*, 773.